THE ASTROPHYSICAL JOURNAL, 373:294–307, 1991 May 20

A CATASTROPHE MECHANISM FOR CORONAL MASS EJECTIONS

T. G. FORBES & P. A. ISENBERG
Institute for the Study of Earth, Oceans, and Space, University of New Hampshire, Durham, NH 03824
Received 1990 August 22; accepted 1990 November 12

ABSTRACT

We use the ideal-MHD equations to show that a coronal current filament can suddenly lose equilibrium if its magnetic energy exceeds a critical value. The loss of equilibrium in our configuration results from an imbalance between magnetic tension and compression, and this imbalance ejects the filament upwards. Near the critical value the equilibrium configuration develops a vertical current sheet attached to the photosphere at the point directly below the filament. When equilibrium is lost, field lines anchored to the photosphere are stretched upwards, and the current sheet rapidly grows longer. Without reconnection in the current sheet, the filament travels only a short distance before reaching a new equilibrium, and the net magnetic energy released is less than 1% of the stored magnetic energy. However, with reconnection, the filament travels upwards indefinitely, and all of the stored energy is released.

Subject headings: hydromagnetics — Sun: corona — Sun: particle emission

1. INTRODUCTION

In 1978, W. Van Tend and M. Kuperus proposed a simple catastrophe model which suggests that a coronal current filament will lose equilibrium when its current exceeds a critical value (Van Tend & Kuperus 1978; Van Tend 1979). During the last few years there has been renewed interest in the model of Van Tend and Kuperus, and several studies have been completed which re-examine the assumptions of the model. The studies by Kaastra (1985), Molodenskii & Filippov (1987), and Martens & Kuin (1989) generalize the model of Van Tend and Kuperus within the framework of circuit theory, while Démoulin & Priest (1988), Amari & Aly (1989), Priest & Forbes (1990), and Anzer & Ballester (1990) develop MHD versions of the model. Here we consider the model of Van Tend and Kuperus within the framework of ideal MHD for a strongly magnetized plasma. Unlike the previous MHD models, our model includes both a current sheet and a current filament of finite radius.

Figure 1 illustrates the basic magnetic mechanism which drives the current filament upwards in the model of Van Tend and Kuperus. In Figure 1*a*, a current filament (*dark shaded region*) is stably suspended above the photosphere (*light shaded region*) because the field lines surrounding the current filament are line-tied to the photosphere. If the filament is perturbed, it simply oscillates up and down around its equilibrium location as indicated in the energy diagram in Figure 1*b*. However, this stable equilibrium is displaced upwards if the current in the filament increases as shown in Figures 1*c* and 1*d*.

Van Tend (1979) showed that a transition like that in Figure 1 can occur either continuously or discontinuously depending on the distribution of the vertical component of the photospheric magnetic field. The vertical component is due to background current sources in the convection zone below the photosphere, and the transition is discontinuous only if the photospheric background field falls off with height faster than $1/y$, where y is the vertical coordinate.

In the analyses by Van Tend & Kuperus (1978) and Molodenskii & Filippov (1987), the current filament is simply treated as a wire immersed in a vacuum, and the magnetic field lines are not frozen to the plasma as they are in ideal MHD. Consequently, reconnection occurs freely at the x-line present in all these models. However, in a realistic plasma environment reconnection is inhibited by the conductivity of the plasma, and any attempt to change a configuration with an x-line in it leads to the formation of a current sheet at the x-line. Kaastra (1985) and Martens & Kuin (1989) addressed this problem by incorporating current sheets within the circuit framework of Van Tend and Kuperus. However, the approximations they use restrict their analyses to situations where the current in the sheet is very much weaker than the current in the filament itself.

If reconnection occurs in the current sheet below the filament, then all the energy is released and the upward motion of the filament is unbounded. The speed at which the current filament moves upwards depends strongly on the rate of reconnection. Observations indicate that some coronal mass ejections (CMEs) move at a speed close to the coronal Alfvén speed, and for these CMEs the reconnection would have to be rapid enough to reconnect a significant fraction of the field within a few Alfvén time scales. Our theoretical understanding of how such rapid reconnection might occur is somewhat limited, but one attractive possibility is that the flows generated by the loss of ideal–MHD equilibrium may act to drive the reconnection rapidly (Forbes 1990). Unlike spontaneous reconnection, driven reconnection is limited only by the Alfvén speed of the system and not by the value of the electrical conductivity (Yeh & Axford 1970; Forbes & Priest 1987).

A current sheet develops during the evolution of a CME because the magnetic field lines above the CME have footpoints anchored in the photosphere, and the field lines become stretched as the ejection moves outwards. In most plasma processes, the formation of a current sheet increases the magnetic energy, but to drive a CME magnetically one needs the magnetic energy to decrease. How a CME creates a current sheet while decreasing the magnetic energy of the system has been an open question (Sturrock 1987; Mikic, Barnes, & Schnack 1988; Biskamp & Welter 1989; van Ballegooijen & Martens 1989).

Aly (1984, 1985, 1990) has argued that for a simply connected force-free field, an open-field configuration is the highest magnetic energy state possible. If Aly is correct, then it is impossible for a simply connected force-free field to produce an open-field configuration by reducing the magnetic energy of the system. Although Aly's theoretical analysis greatly restricts the mechanisms

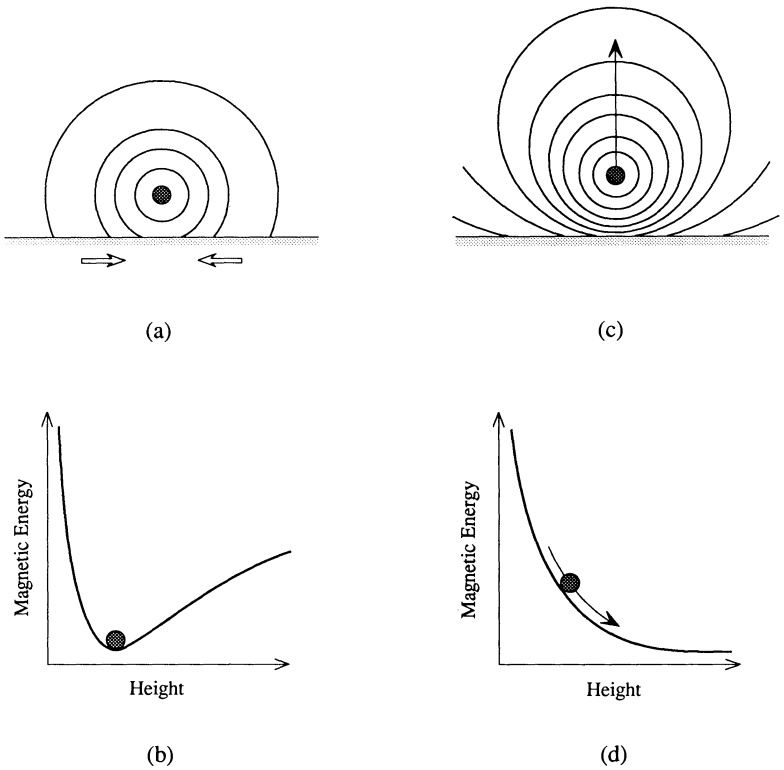

FIG. 1.—Schematic diagram of the driving mechanism in models of the Van Tend and Kuperus type. The shaded circle designates the current filament, and solid arrows indicate filament motions. Hollow arrows show the photospheric convection which increases the filament current by reconnecting field lines in the photosphere.

one might consider for driving CMEs magnetically, there are still several possibilities remaining. First, the initial field configuration in the corona might have current sheets or threads and therefore not be force-free. Second, resistive processes, such as magnetic reconnection, might dissipate the current sheet rapidly enough to eliminate the energy build-up it produces. Third, even if the field is force-free, it may not be simply connected. And fourth, the mass ejection might move from a low-altitude equilibrium to a high-altitude equilibrium without ever opening the field lines to infinity. If the second equilibrium is higher than about two solar radii, then the solar wind will carry the mass ejection into interplanetary space and thereby open the field (Sturrock 1989).

Recently, Klimchuk & Sturrock (1989) have questioned whether a purely force-free field can ever exhibit an MHD catastrophe. Upon re-examining an earlier force-free configuration by Low (1977), they found that the catastrophe-like behavior which occurs in this configuration was an artifact of the solution method used by Low (1977). This has led Sturrock (1989) to speculate that only non-force-free systems can exhibit catastrophic-type behavior.

In the following section we present a two-dimensional analytical model which demonstrates that it is indeed possible for a CME to form an extended field catastrophically, while lowering the magnetic energy of the overall configuration. The model does not contradict the work of either Aly or Klimchuk and Sturrock for two reasons. First, the initial field of the model is neither strictly force-free or simply connected, and second, the field lines, though greatly extended, never become truly open in a mathematical sense.

In the subsequent sections we formulate a model based on a two-stage process. In the first stage, or storage phase, the magnetic energy of the system is slowly increased by transferring magnetic flux from the photosphere to the corona. The transfer of flux occurs quasi-statically over a time period of several days, so that the system evolves through a series of equilibria. The second stage is the eruptive phase which occurs when equilibrium is lost. Immediately after the loss of equilibrium, the system evolves rapidly over a time period of a few minutes (i.e., a few Alfvén time scales). Since the evolution in this stage is very rapid compared to the rate at which flux is transferred from the photosphere to the corona, we consider the flux in the corona to be constant during the eruptive phase. This means there is no external energy input during the eruptive phase.

In § 2 that follows we set up the differential equations for the quasi-static stage of the evolution, and in § 3 we compute the vector potential of the magnetic field. In § 4 we solve for the equilibria and then determine their stability by using an energy analysis in § 5. In general, the equilibria can be found only by numerically solving coupled transcendental equations. However, in § 6 we present an asymptotic analysis which gives simple analytical expressions in the limit of small filament radius. In § 7, we discuss the physical implications of the solutions in relation to observations, and finally in § 8 we summarize our principal results.

2. FORMULATION OF THE MAGNETOHYDRODYNAMIC MODEL

During the quasi-static stage of the evolution, the coronal magnetic field $\boldsymbol{B}$ and current density $\boldsymbol{j}$ are determined by the magnetohydrostatic equations

$$\frac{\boldsymbol{j} \times \boldsymbol{B}}{c} = \nabla p \,, \tag{1}$$

$$\nabla \times \boldsymbol{B} = \frac{4\pi}{c} \boldsymbol{j} \,, \tag{2}$$

$$\nabla \cdot \boldsymbol{B} = 0 \,, \tag{3}$$

where p is the plasma pressure, and c is the speed of light. We assume the pressure in the corona is zero except where the current filament is located. This assumption is often called the strong magnetic field approximation, and in two dimensions it causes all currents to become concentrated into thin line currents or sheets if there is no magnetic field component perpendicular to the two-dimensional plane (see Syrovatskii 1971). The pressure inside the filament is kept finite to prevent the current filament from becoming infinitely thin and the magnetic energy from becoming infinitely large.

Since the driving force in a Van & Tend and Kuperus type model is strictly magnetic, we will neglect gravity. Although gravity may play some role in the propagation of a CME in the outer corona, it is unlikely to be the main driving force since the gravitational potential energy of the pre-existing structure is estimated to be much less than the 10^{32} ergs needed for a large CME (Low 1981; Wagner et al. 1981; Yeh 1982).

We start by assuming that the magnetic field lies in the x-y plane, and that all quantities are invariant in the z direction perpendicular to this plane. Force and energy are determined per unit length except in § 7 where we multiply the energy per unit length by a length scale in the z-direction in order to compare our results to observations.

The total force per unit length on the filament is

$$\boldsymbol{F}_{\rm tot} = \frac{1}{c} \iint_S (\boldsymbol{j}_f \times \boldsymbol{B}_f) da + \frac{1}{c} \iint_S (\boldsymbol{j}_f \times \boldsymbol{B}_e) da - \oint_C p \hat{\boldsymbol{n}} \, dl \,, \tag{4}$$

where S is the region occupied by the filament, a is the area of S, C is the perimeter of S, l is the length of C, $\boldsymbol{j}_f$ is the filament current density, and $\boldsymbol{B}_f$ and $\boldsymbol{B}_e$ are the magnetic fields due to the internal current of the filament and the external currents outside the filament, respectively. We assume a is small enough to make the external field $\boldsymbol{B}_e$ effectively uniform within the filament. With this assumption, the condition for filament equilibria dissociates into two separate conditions—one for the internal, local equilibrium given by

$$\boldsymbol{j}_f \times \boldsymbol{B}_f = c \nabla p \,, \tag{5}$$

and one for the external, global equilibrium given by

$$\boldsymbol{F} = (I B_e^* / c) \hat{\boldsymbol{y}} = 0 \,, \tag{6}$$

where $\boldsymbol{F}$ is the external force per unit length, $\boldsymbol{B}_e^*$ is the external field evaluated at the filament, and I is the filament current

$$I = \iint_S j_f \, da \,. \tag{7}$$

The force referred to in equation (6), is sometimes called a diamagnetic force (Yeh 1983), and this force vanishes when

$$B_e^* = 0 \,. \tag{8}$$

Conservation of mass and flux within the filament determines the distribution of current density, $\boldsymbol{j}_f$, when they are combined with an adiabatic equation of state of the form

$$p \rho^{-\gamma} = \text{constant} \,. \tag{9}$$

Generally, a change in the filament current causes the filament to expand or contract, but in the solutions that follow we will assume that the filament is incompressible ($\gamma \to \infty$) and that the filament radius, r, is constant. Since we have already assumed the plasma to be highly compressible outside the filament, this assumption means there must be an abrupt change in state at the surface of the filament.

To determine the global equilibria prescribed by equation (8), we must first determine the total magnetic field configuration. We do this by solving Poisson's equation for the magnitude of the vector potential A

$$\nabla^2 A = -\frac{4\pi}{c} j(x, y) \,, \tag{10}$$

where $\boldsymbol{B} = \nabla A \times \hat{\boldsymbol{z}}$. At the start of the quasi-static evolution we assume $j(x, y)$ to describe a cylinder of constant radius r and uniform current density $I_i/(\pi r^2)$

$$j(x, y) = \frac{I_i}{\pi r^2} \left[\!\left[1 - \mathscr{H}\{\sqrt{[x^2 + (y - h_i)^2]} - r\} \right]\!\right] \,, \tag{11}$$

where I_i is the initial filament current, h_i is the initial filament height, and $\mathscr{H}$ is the Heaviside step-function. As the system evolves, the current density within the filament remains fixed, and a surface current appears on the filament boundary.

For the photospheric boundary condition we choose

$$A(x, 0) = \frac{md}{x^2 + d^2} - \phi(t) . \tag{12}$$

where m and d are constants and $\phi(t)$ is a slowly varying function of time. This boundary condition is the same as that produced by a line dipole of strength m at a depth d below the photosphere. We choose a line dipole to represent the boundary field because in a multipole expansion of an arbitrary boundary field, the line-dipole term is the first term which allows a catastrophe to occur (Van Tend 1979; Démoulin & Priest 1988).

We will consider the quasi-static evolution of MHD equilibria caused by the gradual reconnection of photospheric field lines below the filament. The reconnection transfers the flux, ϕ, from the photosphere to the corona and leads to the storage of magnetic energy. For convenience we choose a photospheric flow pattern which transports new field lines from $x = \pm\infty$ so as to maintain the same distribution of normal magnetic field in the photosphere. This choice requires the tangential flow velocity at the photospheric boundary to be

$$v_x(x, 0) = -\frac{(x^2 + d^2)}{2md\,x}\frac{d\phi}{dt} , \tag{13}$$

which transports field lines to the origin where they are reconnected. Such a flow pattern is not especially realistic, but it is mathematically convenient for illustrating the principle of current filament formation by photospheric reconnection.

It may at first seem paradoxical that magnetic reconnection can store magnetic energy in the corona, since reconnection is usually invoked in flare models as a way to release magnetic energy. However, the reconnection process we envision here is analogous to the energy storage process that occurs in the Earth's magnetosphere prior to an auroral substorm. In that context, sustained reconnection at the dayside magnetopause transfers energy from the solar wind to the magnetotail. Magnetic energy is thereby stored in the magnetotail prior to the onset of the substorm, and when the substorm starts, this stored energy is quickly dissipated by rapid reconnection in the central current sheet of the magnetotail (Hones 1979).

3. SOLUTION FOR THE VECTOR POTENTIAL

As we will see, evolution through the stable equilibria eventually causes a vertical current sheet to appear along the y-axis. Prior to the formation of this current sheet, the solution is relatively simple, and we obtain it by using the method of images. However, after the current sheet appears, the solution is more complicated, and we use conformal mapping and the method of Green functions to obtain it.

3.1. *Solution Before Current Sheet Forms*

Prior to the formation of the current sheet, the filament is the only current source in the region $y > 0$, and initially this source is prescribed by equation (11). As the system evolves, the distribution of current within the filament changes, but since the filament radius is small, the magnetic field is approximately the same as that produced by a line current of strength I at the location $y = h$. That is

$$j(x, y) = I\,\delta(x)\delta(y - h) , \tag{14}$$

as long as $|y - h| \gg r$.

The method of images gives a simple solution to equations (10), (12), and (14) of the form

$$A(x, y) = \frac{2I_0}{c}\,\mathrm{Re}\left[J \ln\left(\frac{\zeta + ih}{\zeta - ih}\right) + \frac{2i}{\zeta + i}\right] - \phi , \qquad \text{for } |\zeta| \gg r , \tag{15}$$

where $\zeta = x + iy$ is the complex coordinate, $I_0 = m/2d$, $J = I/I_0$, and x, y, h, and r are now normalized to the length scale, d. The field (15) is equivalent to that produced by a line current, JI_0 at $\zeta = ih$, an image line current, $-JI_0$ at $\zeta = -ih$, and a line dipole of strength $2dI_0$ at $\zeta = -i$. The image current and the dipole are the sources for the field, B_e, external to the filament.

The magnetic field along the y-axis is

$$B_x(0, y) = \frac{2I_0}{dc}\left[\frac{J}{y + h} - \frac{J}{y - h} - \frac{2}{(y + 1)^2}\right] \tag{16}$$

and the corresponding flux between the filament and the photosphere is

$$\phi = (2I_0/c)\{J \ln[(2h/r) - 1] - 2(h - r)/(h - r + 1)\} , \tag{17}$$

for any value of $h > r$. Simultaneous solution of equations (15) and (17) determine the potential, A, and the filament current, J, as functions of the filament height, h, and the reconnected flux, ϕ.

Setting $B_x(0, 0) = 0$ in equation (16) shows that the x-line first appears when $h = 1$ and $J = 1$. Since a current sheet forms immediately after the appearance of the x-line, we define the point $h = h_0$, $\phi = \phi_0$ in the $h - \phi$ plane as the sheet formation point, where from equation (17)

$$\phi_0 = \left(\frac{2I_0}{c}\right)\left\{\ln\left[\left(\frac{2}{r}\right) - 1\right] - 2\,\frac{(1 - r)}{(2 - r)}\right\} . \tag{18}$$

and $h_0 = 1$.

3.2. *Solution After Current Sheet Forms*

To determine the magnetic field configuration after the appearance of the current sheet, we use a conformal mapping which transforms the current sheet into a line segment collinear with the photosperic boundary. In the absence of reconnection in the corona, the current sheet is always attached to the photosphere, and so the conformal mapping which accomplishes this transformation is simply

$$w = \sqrt{\zeta^2 + q^2}\,, \tag{19}$$

where $w = u + iv$ and q is the normalized length of the current sheet as illustrated in Figure 2.

In the $u-v$ plane we have

$$\nabla^2 A = -\frac{4\pi j(u, v)}{c}\,, \tag{20}$$

$$j(u, v) = (I_0/d^2)J\,\delta(u)\delta(v - \sqrt{h^2 - q^2})\,, \tag{21}$$

with the boundary condition

$$A(u, 0) = -\phi(t) + \frac{4I_0}{c}\begin{cases} 1 & u^2 \le q^2\,, \\ (u^2 - q^2 + 1)^{-1} & u^2 > q^2\,. \end{cases} \tag{22}$$

The general form of solution for equation (20) is

$$A(u, v) = \frac{1}{c}\int_0^\infty \int_{-\infty}^\infty j(u', v')G(u, v, u', v')du'\,dv' + \frac{1}{4\pi}\int_{-\infty}^\infty A(u', 0)\left.\frac{\partial G(u, v, u', v')}{\partial v'}\right|_{v'=0} du'\,, \tag{23}$$

where $G(u, v, u', v')$ is the two-dimensional Green function

$$G(u, v, u', v') = \ln\left[\frac{(u - u')^2 + (v + v')^2}{(u - u')^2 + (v - v')^2}\right]. \tag{24}$$

Substitution of equations (21), (22), and (24) into equation (23) gives

$$\begin{aligned} A(u, v) = {} & \frac{I_0 J}{c}\ln\left[\frac{u^2 + (v + \sqrt{h^2 - q^2})^2}{u^2 + (v - \sqrt{h^2 - q^2})^2}\right] + \frac{4I_0}{\pi c^2}\int_{-\infty}^{-q}\frac{v\,du'}{[(u - u')^2 + v^2](u'^2 - q^2 + 1)} \\ & + \frac{4I_0}{\pi c}\int_{-q}^{q}\frac{v\,du'}{(u - u')^2 + v^2} + \frac{4I_0}{\pi c}\int_q^\infty \frac{v\,du'}{[(u - u')^2 + v^2](u'^2 - q^2 + 1)} - \phi(t)\,, \end{aligned} \tag{25}$$

which is the real part of the complex potential $\mathscr{A}(w)$

$$\begin{aligned} \mathscr{A}(w) = {} & \frac{2I_0 J}{c}\ln\left(\frac{w + i\sqrt{h^2 - q^2}}{w - i\sqrt{h^2 - q^2}}\right) + i\frac{4I_0}{\pi c}\int_{-\infty}^{-q}\frac{dt}{(t^2 - q^2 + 1)(w - t)} \\ & + i\frac{4I_0}{\pi c}\int_{-q}^{q}\frac{dt}{(w - t)} + i\frac{4I_0}{\pi c}\int_q^\infty \frac{dt}{(t^2 - q^2 + 1)(w - t)} - \phi(t)\,. \end{aligned} \tag{26}$$

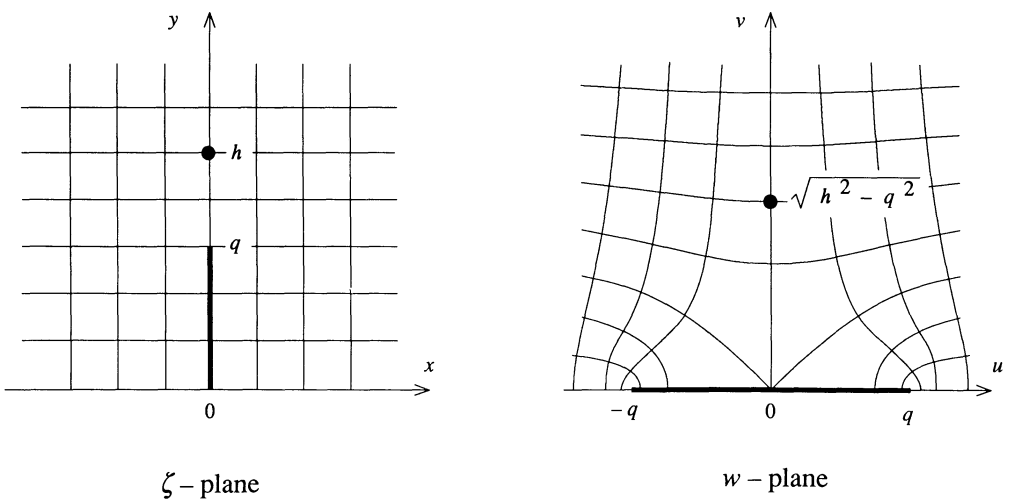

FIG. 2.—Conformal mapping of the ζ-plane to the w-plane. The quantities h and q are the filament height and current sheet length, respectively.

After substitution of equation (19) and evaluation of the integrals, the real potential in the x-y plane is

$$A(x, y) = \frac{2I_0}{c}\,\mathrm{Re}\left[J\ln\left(\frac{\sqrt{\zeta^2+q^2}+i\sqrt{h^2-q^2}}{\sqrt{\zeta^2+q^2}-i\sqrt{h^2-q^2}}\right)+\frac{2i\zeta^2}{\pi(\zeta^2+1)}\ln\left(\frac{\sqrt{\zeta^2+q^2}+q}{\sqrt{\zeta^2+q^2}-q}\right)\right.$$
$$\left.+\frac{2}{\zeta^2+1}+\frac{2i}{\pi\sqrt{q^2-1}}\,\frac{\sqrt{\zeta^2+q^2}}{\zeta^2+1}\ln\left(\frac{q+\sqrt{q^2-1}}{q-\sqrt{q^2-1}}\right)\right]-\phi(t)\,. \tag{27}$$

For $q < 1$ in equation (27), the expression $\ln\{[q+(q^2-1)^{1/2}]/[q-(q^2-1)^{1/2}]\}/(q^2-1)^{1/2}$ can be replaced by $-(2/\pi)\{\tan^{-1}[q/(1-q^2)^{1/2}]-1\}/(1-q^2)^{1/2}$. When $q=0$, equation (27) reduces to equation (15), the corresponding equation for the no-current-sheet regime.

To complete the solution for A, we need to determine q and J as functions of the reconnected flux ϕ. We first determine q as a function of h and J by setting the transverse field at the top of the current sheet to zero. That is

$$B_x(0, q) = 0\,. \tag{28}$$

This condition forces the field to have a y-point configuration at the top of the current sheet. Since the magnetic field along the y-axis is

$$B_x(0, y) = \frac{1}{d}\frac{\partial A}{\partial y} = \frac{2I_0}{dc}\left[\frac{2Jy\sqrt{h^2-q^2}}{(h^2-y^2)\sqrt{y^2-q^2}}-\frac{4y}{\pi(y^2-1)^2}\tan^{-1}\left(\frac{2q\sqrt{y^2-q^2}}{y^2-2q^2}\right)\right.$$
$$\left.-\frac{4yq}{\pi(y^2-1)\sqrt{y^2-q^2}}+\frac{4y}{(y^2-1)^2}-\frac{2y(y^2-2q^2+1)}{\pi(y^2-1)^2\sqrt{(q^2-1)(y^2-q^2)}}\ln\left(\frac{q+\sqrt{q^2-1}}{q-\sqrt{q^2-1}}\right)\right], \tag{29}$$

equation (28) requires that

$$\frac{J}{\sqrt{h^2-q^2}}-\frac{2q}{\pi(q^2-1)}+\frac{1}{\pi(q^2-1)^{3/2}}\ln\left(\frac{q+\sqrt{q^2-1}}{q-\sqrt{q^2-1}}\right)=0\,. \tag{30}$$

Figure 3 shows some examples of the field configurations with and without current sheets.

Next, we determine the reconnected flux, ϕ, between the photosphere and the filament as a function of J. This flux is just the difference between A at the surface of the filament and A at the photosphere, i.e.,

$$\phi = A(0, h-r) - A(0, 0)\,. \tag{31}$$

Equation (31) still holds when the current sheet is present since the value of A along the current sheet is constant and equal to $A(0, 0)$. Thus, for $r \ll h$

$$\phi = \frac{2I_0}{c}\left\{J\ln\left[\frac{2(h^2-q^2)}{hr}\right]+\frac{2h^2}{\pi(h^2-1)}\tan^{-1}\left(\frac{2q\sqrt{h^2-q^2}}{h^2-2q^2}\right)-\frac{2h^2}{h^2-1}+\frac{2\sqrt{h^2-q^2}}{\pi(h^2-1)\sqrt{q^2-1}}\ln\left(\frac{q+\sqrt{q^2-1}}{q-\sqrt{q^2-1}}\right)\right\}. \tag{32}$$

Equations (6), (29), (30), and (32) are not exact since we used a far-field approximation to derive them. The largest error occurs in equation (32), the expression for the flux, since we obtained this expression by integrating the total field over a region which includes the region near the filament where the total field is not accurately represented by equation (29). However, one can show that the net error in the flux is of second order in the small parameter r/h and that equation (32) is therefore accurate to first order in r/h.

4. EQUILIBRIA

In this section we compute the force on the filament and obtain the equilibria by finding the positions where the force is zero. In the subsequent section (§ 5) we will determine the total magnetic energy of the system by integrating the force with height, and then use the result to determine the stability of the equilibria with respect to vertical motions.

From equation (6) the force per unit length is

$$\boldsymbol{F} = \frac{I_0}{c}\,J\lim_{y\to h}\left[B_x(0, y)+\frac{2I_0 J}{dc(y-h)}\right]\hat{\boldsymbol{y}}\,, \tag{33}$$

where the last term subtracts the self-field of the filament. Prior to the formation of a current sheet the field $B_x(0, y)$ is given by equation (16), and the magnitude of the force on the filament is

$$F = \frac{2I_0^2}{dc^2}\,J\left[\frac{J}{2h}-\frac{2}{(h+1)^2}\right]. \tag{34}$$

Setting $F = 0$ we find that the equilibria occur at

$$h = (2 - J - 2\sqrt{1-J})/J\,, \tag{35}$$

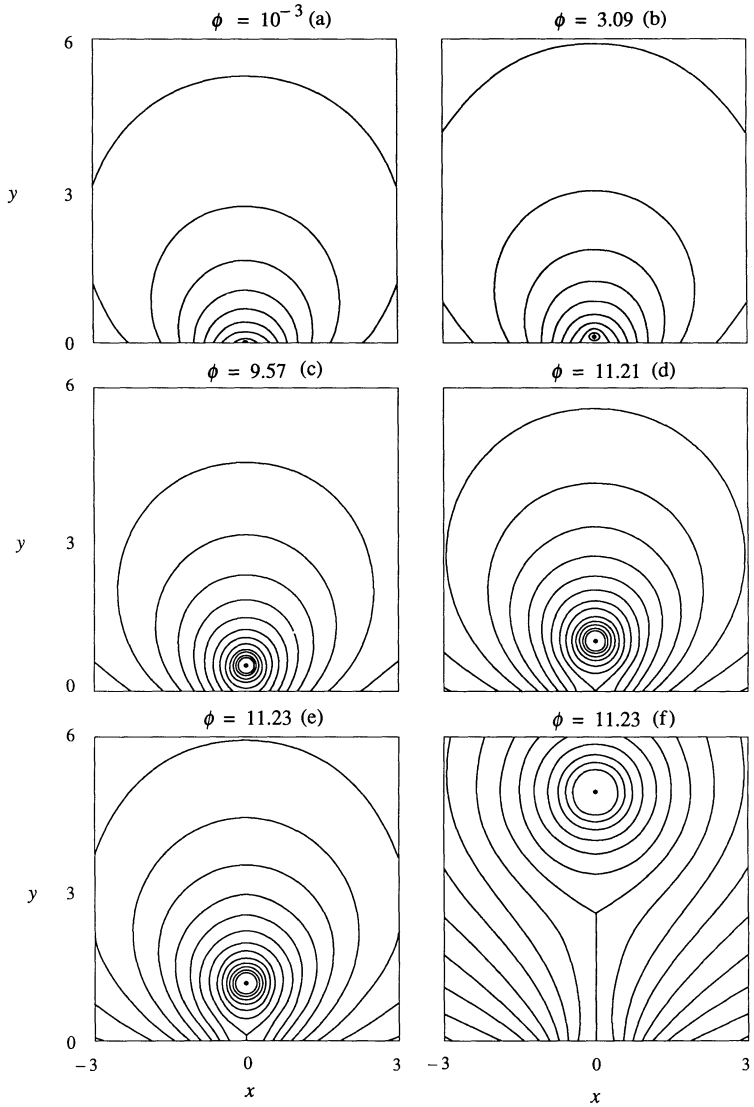

FIG. 3.—Contours of the vector potential for a normalized filament radius of 10^{-5}. The six different configurations, labeled (*a*) through (*f*), correspond to different locations on the equilibrium curve. The contour levels are not the same for all panels, and the field lines near the current filament are omitted. The parameter ϕ is the flux between the filament and the base in units of $2I_0/c$, and at $\phi = 10^{-3}$ in (*a*) the dipole background field completely dominates. Reconnection in the photosphere causes ϕ to continually increase in (*b*) and (*c*), and this increase eventually leads to the formation of a neutral line in (*d*) and a current sheet in (*e*). However, when ϕ reaches 11.23 the equilibrium height jumps discontinuously from $h = 1.11$ to $h = 4.90$ as shown in (*e*) and (*f*).

where from equation (17)

$$\phi = (2I_0/c)[J \ln(2h/r) - 2h/(h+1)] , \tag{36}$$

for $r \ll h$ (see Forbes 1990).

After the current sheet appears the field $B_x(0, y)$ is given by equation (29), and the force is

$$F = \frac{2I_0^2 J}{dc^2}\left[\frac{J(h^2+q^2)}{2h(h^2-q^2)} - \frac{4h}{\pi(h^2-1)^2}\tan^{-1}\left(\frac{2q\sqrt{h^2-q^2}}{h^2-2q^2}\right) - \frac{4qh}{\pi(h^2-1)\sqrt{h^2-q^2}}\right.$$
$$\left. + \frac{4h}{(h^2-1)^2} - \frac{2h(h^2-2q^2+1)}{\pi(h^2-1)^2\sqrt{(q^2-1)(h^2-q^2)}}\ln\left(\frac{q+\sqrt{q^2-1}}{q-\sqrt{q^2-1}}\right)\right] . \tag{37}$$

Equilibria occur when $F = 0$ in (37) where q and J are given by equations (30) and (32). We solve these coupled equations numerically using a standard algorithm (Wolfram 1988) and obtain solutions as functions of ϕ and r. As an illustrative example, we set $r = 10^{-5}$ and show the solutions for A, h, and J in Figures 3, 4, and 5. Figure 4 shows there is a single solution for any given value of the flux ϕ except for the small range of flux between 11.05 and 11.23. In this range the solution is multivalued, and it is here where catastrophe behavior is possible.

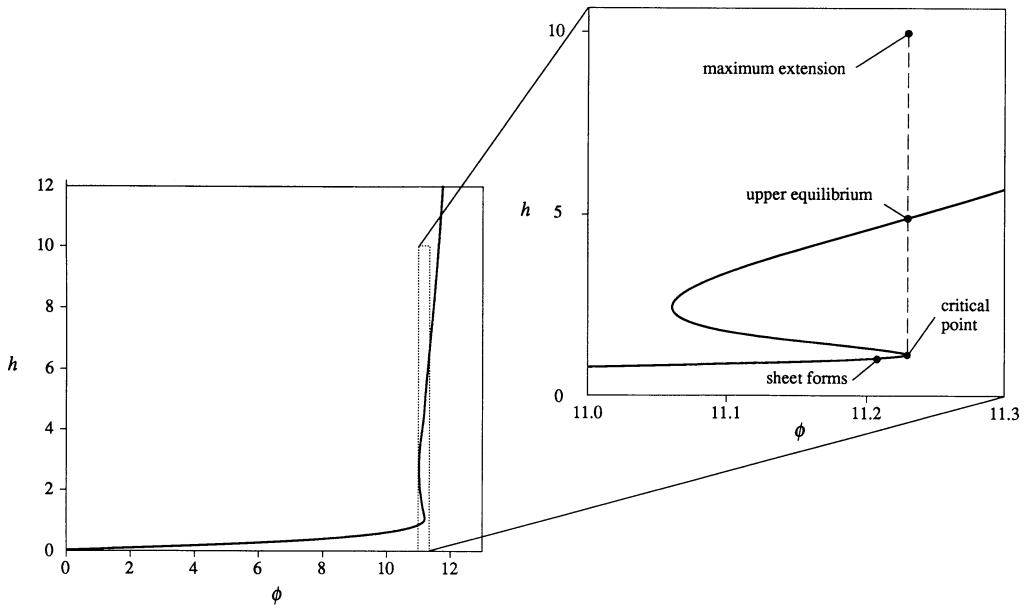

FIG. 4.—Normalized equilibrium height h as a function of the reconnected flux ϕ for $r = 10^{-5}$. The plot at right is a blow-up of the dotted rectangular region in the left plot. As the reconnected flux ϕ increases, the filament moves along the lower branch of the equilibrium curve towards the critical point, and when the critical point is reached the filament is ejected upwards. Without dissipation, the filament would oscillate between the critical point and the maximum extension height.

Figure 3 shows six different field configurations corresponding to six different stages in an evolutionary sequence along the equilibrium curve in Figure 4. The configurations in Figures 3*a* through 3*e* show the quasi-static evolution along the equilibrium curve from a nearly potential configuration at $\phi = 10^{-3}$ (Fig. 3*a*) to the catastrophe-point configuration at $\phi = 11.23$ (Figure 3*e*). The sequence starts with $\phi = 10^{-3}$ instead of 0, because our solution is not valid at $\phi = 0$. At $\phi = 0$, equation (17) gives $h = r$, contrary to our assumption that $h \gg r$.

The configuration in Figure 3*a* has $h = 10r$ and $J = 4 \times 10^{-4}$. This value of J is so small that the field is essentially identical to the potential field when no filament is present. However, the presence of the small current filament is essential for the subsequent evolution of the field. If no current filament is present initially, field lines moving towards the origin disappear by submerging, and the coronal field remains potential. The presence of a filament prevents this because it reverses the sign of the tangential magnetic field component, $B_x(0, 0)$, and this reversal means that field lines emerge, rather than submerge (see van Ballegooijen & Martens 1989).

At $\phi = 11.21$ an x-line appears at the origin, and a current sheet forms as ϕ increases beyond this value. The ideal–MHD

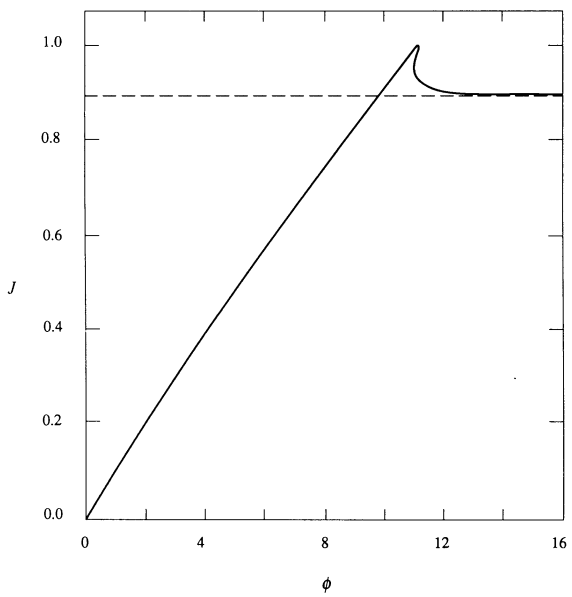

FIG. 5.—Normalized equilibrium current J as a function of the reconnnected flux ϕ for $r = 10^{-5}$. The dashed line shows the asymptotic value of J as h tends to infinity.

TABLE 1

EQUILIBRIUM PROPERTIES AT THE CRITICAL POINT TRANSITION

Filament Radius r	Lower Height h_c	Upper Height h_u	Lower Length q_c	Upper Length q_u	Lower Energy W_c	Upper Energy W_u	Energy Released $(W_c - W_u)/W_c$
10^{-3}				No critical point is present			
10^{-5}	1.114	4.90	0.088	2.51	6.127	6.114	0.21%
10^{-7}	1.074	9.93	0.057	5.51	8.421	8.398	0.28
10^{-9}	1.054	18.4	0.042	10.5	10.720	10.677	0.40
$10^{-\infty}$	1.000	∞	0.000	∞	∞	∞	0.99

equations do not permit reconnection in the corona, and thus there is no reconnection in the current sheet except at the point where it is attached to the photosphere. Because the current sheet is infinitely thin, the flux reconnected at its photospheric base immediately appears at the top of the current sheet. The point at which the x-line forms is labeled in Figure 4, and this is the point we defined in § 3.1 as the sheet-formation point.

At $\phi = 11.23$ the equilibrium curve in Figure 4 reaches a critical point where the lower branch of the solution vanishes, and for $\phi > 11.23$ only the upper branch remains. Figures 3*e* and 3*f* show the two field configurations corresponding to the lower and upper branches of the equilibrium curve at this critical point.

We define the reconnected flux and the filament height at the critical point as ϕ_c and h_c, respectively. At the critical point the system undergoes an abrupt transition from the lower to the upper equilibrium as indicated in Figure 4. As we will show shortly, this sudden transition is due to a true loss of mechanical equilibrium and not to any limitation of our method of solution (see Klimchuk & Sturrock 1989).

Figure 5 shows that the filament current J increases as the reconnected flux increases. The current reaches its maximum value of unity at the sheet-formation point ($h_0 = 1$, $\phi_0 = 11.21$), rather than at the critical point ($h_c = 1.114$, $\phi_c = 11.23$). As the flux increases beyond ϕ_0, the current decreases to an asymptotic value of 0.900 (see § 6). The decrease in filament current means that the magnetic energy added after the current sheet forms is stored in the current sheet field rather than in the filament field.

Table 1 shows how the equilibrium heights at the critical point transition vary with the filament radius. As the radius tends to zero, the lower equilibrium height approaches unity while the upper equilibrium height approaches infinity. On the other hand, as the radius becomes larger, the lower and upper equilibrium heights approach each other, and at a radius of about $r = 10^{-3}$, they meet and disappear. If the filament radius exceeds 10^{-3} times the photospheric length scale, d, there is no longer a catastrophe in this model.

5. ENERGETICS AND STABILITY

The stability of the equilibria to upward motion is easily obtained by evaluating the force as a function of filament height under the condition that the flux ϕ remains constant. Simultaneously solving equations (30), (32), and (37) gives the force as a function of height for a given flux. For example, Figure 6 shows the force as a function of height for $r = 10^{-5}$ and $\phi = \phi_0$, the flux when the current sheet first appears. In this case there are three different heights where the force is zero, and these three heights corresponds to the three branches of the equilibrium curve at $\phi = \phi_0$ in Figure 4. The lowest and highest equilibria at $h = 1$ and $h = 4.9$ are stable since the force that results from a small displacement opposes the displacement. However, the middle equilibrium height at $h = 1.1$ is unstable since here the force enhances the displacement.

If the filament is moved downwards from its starting position at $h = 1$, our solution no longer applies because a curved current sheet forms as field lines are compressed between the filament and the photosphere. However, since the field lines are compressed we expect the force to be positive as indicated by the dotted line in Figure 6.

To calculate the energy changes during the evolution of the system we consider the incremental work dW (per unit length) required to displace the filament a distance ds and to change the flux by an amount $d\phi$

$$dW(s, \phi) = \frac{\partial W}{\partial s}\, ds + \frac{\partial W}{\partial \phi}\, d\phi \,. \tag{38}$$

Setting the displacement $s = hd$, we recognize that $2W/2s = d2W/2h = -Fd$ and $2W/2\phi = I/c$. Then the net change in magnetic energy due to the work done on the filament is

$$\Delta W(h, \phi) = -d \int_C F(h, \phi)\, dh + \frac{1}{c} \int_C I(h, \phi)\, d\phi \,, \tag{39}$$

where C is a path of integration in the $h - \phi$ plane. The first term on the right-hand side of equation (39) is the change in magnetic energy due to the displacement of the filament, while the second term is the change in magnetic energy due to the variation of the flux in the circuit (see Reitz & Milford 1960). Since changes in flux are caused only by photospheric reconnection, the second term on the right-hand side of equation (39) is just the work done by the photospheric convection.

The energy change per unit length associated with a vertical displacement of the filament from the height, h_0, is

$$\Delta W = -d \int_{h_0}^{h} F(h', \phi)\, dh' \,, \tag{40}$$

if the flux is constant during the displacement. We can also evaluate the change in energy for points along the equilibrium curve by

simply integrating along it, i.e.,

$$\Delta W(\phi) = \frac{I_0}{c} \int_{\phi_0}^{\phi} J[h(\phi'), \phi'] \, d\phi' \,, \tag{41}$$

where ϕ_0 is fhe flux at the point on the equilibrium curve where the current sheet first appears (the sheet formation point). The function $J[h(\phi'), \phi']$ is determined from the coupled equations (30), (32), and (37) with $F = 0$.

Because the line integrals in equation (39) are path-independent, the change in energy between any points in the h-ϕ plane must be the same for all paths of integration between the two points. We have taken advantage of this property to check our numerical procedures and have found the numerical integrations errors to be less than 10^{-6}.

To interpret our results physically, we define W, the absolute energy per unit length, to be

$$W = \Delta W + W_0 \,, \tag{42}$$

where

$$W_0 \equiv \frac{2I_0^2}{c^2} \int_1^{\infty} J(h') \left[\frac{J(h')}{2h'} - \frac{2}{(h' + 1)^2} \right] dh' \,. \tag{43}$$

The current $J(h')$ is determined from the constant-flux condition by setting $\phi = \phi_0$ in equations (17) and (18) to give

$$J(h) = \frac{\ln [(2/r) - 1] - [2(1 - r)/(2 - r)] + [2(h - r)/(h - r + 1)]}{\ln [(2h/r) - 1]} \,. \tag{44}$$

The constant W_0 is the stored magnetic energy available for driving the filament when reconnection is allowed. The first term in (43)

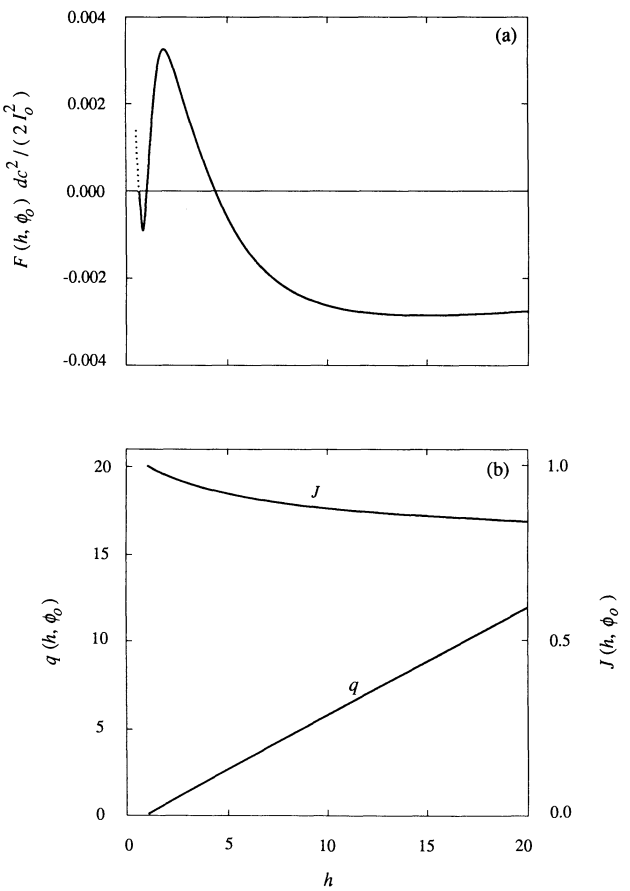

FIG. 6

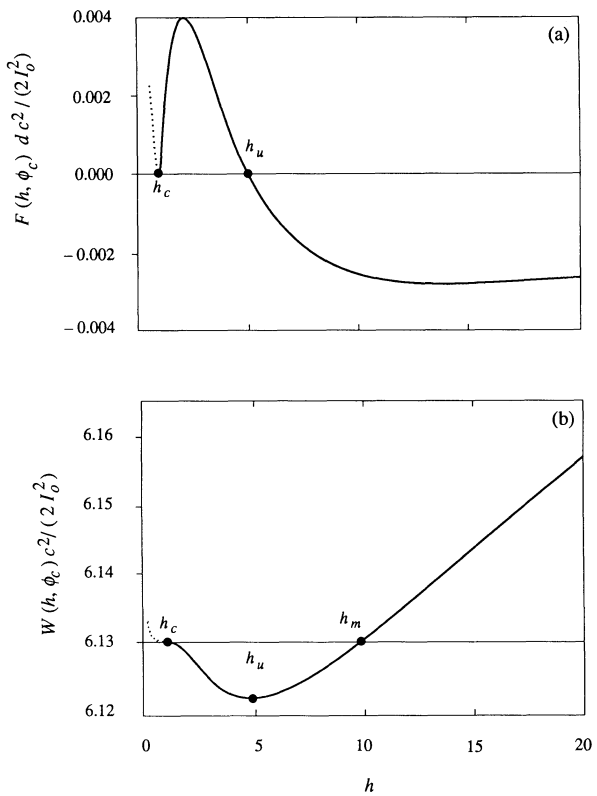

FIG. 7

FIG. 6.—(*a*) Force, F, on the filament as a function of height for constant flux ϕ_0. Here the normalized filament radius, r, is 10^{-5}, and $\phi_0 = 11.21$. (*b*) Filament current, J, and the current sheet length, q, as functions of the filament height h. The dotted extension of the curve to the left shows the expected variation when the filament is moved downwards from the critical point.

FIG. 7.—Force (*a*) and magnetic energy (*b*) as functions of filament height for constant critical flux ϕ_c. The normalized filament radius is $r = 10^{-5}$, and the critical flux is $\phi_c = 11.23$. The heights h_c, h_u, and h_m are the filament heights at the critical point, the upper equilibrium, and the maximum extension, respectively. The dotted extension of the curve to the left shows the expected variation when the filament is moved downwards from the critical point.

is the magnetic energy associated with the repulsive force between the filament and its image, while the second term is the magnetic energy associated with the attractive force between the filament and the photospheric background field. With this definition for W_0, zero magnetic energy occurs when the coronal currents vanish as happens in our model when the current sheet is dissipated by reconnection. When the current sheet is dissipated, the filament moves to infinity, and the filament current decreases to zero.

Figure 7 plots the force $F(h, \phi_c)$ and energy $W(h, \phi_c)$ as functions of height for constant critical flux, ϕ_c. At the critical point ($h = h_c$), the force on the filament is zero, but when the filament is moved upwards, the force is greater than zero until the filament reaches the upper equilibrium height h_u where the force is again zero. Beyond h_u, the force is negative, and its magnitude increases without bound as h approaches infinity. The associated energy curve shows that the upper equilibrium height, h_u, corresponds to the minimum of a potential well, and that h_c corresponds to an inflection point at the lower edge of the well. Thus, an infinitesimal perturbation of a filament initially at h_c will launch the filament upwards towards h_u. If the filament continues to move upwards beyond h_u, the magnetic energy starts to increase, and it becomes equal to the initial magnetic energy again when $h = h_m$. Thus, h_c and h_m are the boundaries of the potential well in which the filament oscillates unless its energy is dissipated. If the filament energy is dissipated, then the filament comes to rest at the upper equilibrium height, h_u.

We numerically solve equations (37), (40), (42), and (43) to obtain the equilibrium filament height as a function of the stored energy at any phase in the evolution. Figure 8 shows the result for the particular case where $r = 10^{-7}$. When the stored magnetic energy exceeds the value of 8.4 times $2I_0^2/c^2$, the filament suddenly jumps upwards along the dotted curve which is obtained from setting $\phi = \phi_c$ in equations (30), (32), and (42). As the filament moves along this curve its energy decreases slightly, until it reaches the upper equilibrium at $h = 9.9$. If there is no reconnection and if the filament motion is quickly damped, then the filament comes to rest at the upper equilibrium. Increasing the stored energy yet further, leads to a continued rise in filament height, but at a rate which is very much faster than the rate prior to the formation of the current sheet.

Table 1 shows how the equilibrium energies at the critical point transition vary with the filament radius. As the radius tends to zero, both the lower and upper equilibrium energies approach infinity, but the percentage of magnetic energy released, relative to the total energy stored, approaches only 0.99% (see § 6).

Anzer & Ballester (1990) have shown that the catastrophe behavior in the CME model of Démoulin & Priest (1988) also disappears when the filament radius exceeds a specific value. Anzer & Ballester (1990) did not determine this value exactly, but they did show that it is less than 10^{-6} times the photospheric length-scale. The limiting radius in the Démoulin & Priest (1988) configuration is at least three orders of magnitude smaller than the limiting radius in our model. This three orders of magnitude difference is probably due to the quite different configuration of the Démoulin & Priest (1988) solution which has no current sheet, and has periodic boundary conditions and a linear force-free field exterior to the filament.

6. ASYMPTOTIC SOLUTION FOR SMALL RADIUS

As the filament radius, r, tends to zero, the upper equilibrium height, h_u, tends to infinity. When h is large, equations (30), (32), and (37) simplify, and we can get analytical results without resorting to numerical methods. For $h \to \infty$ and $\phi = \phi_0$, these equations reduce to

$$h^2 = [(\pi/2)^2 J^2 + 1] q^2 , \tag{45}$$

$$J = \frac{\ln(2/r) + 1 - 2\pi^{-1} \tan^{-1} [(2q\sqrt{h^2 - q^2})/(h^2 - 2q^2)]}{\ln [2(h^2 - q^2)/(hr)]} , \tag{46}$$

$$F(h) = \frac{2I_0^2}{dc^2} J \left[\frac{J(h^2 + q^2)}{2h(h^2 - q^2)} - \frac{4q}{\pi h \sqrt{h^2 - q^2}} \right] . \tag{47}$$

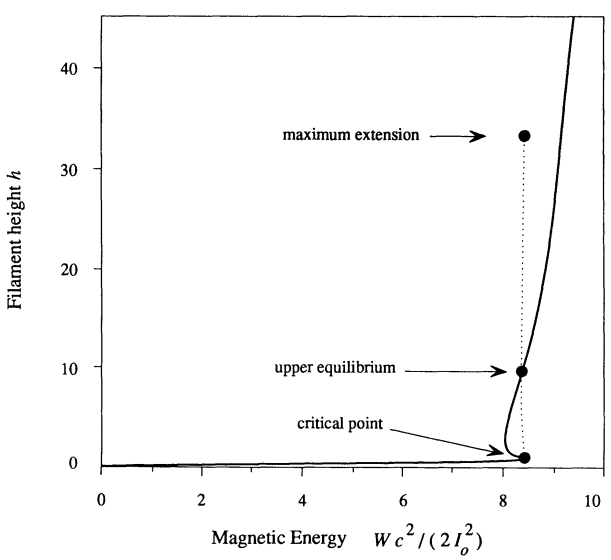

FIG. 8.—Equilibrium filament height as a function of stored magnetic energy. The dashed curve is the expected filament trajectory when the system reaches the critical point, and the maximum extension is the maximum height reached by the filament in the absence of any dissipation or reconnection.

The critical point approaches the sheet formation point as $r \to 0$, so h_0 and ϕ_0 are approximately equal to h_c amd ϕ_c. Thus in the limit that r tends to zero and h tends to infinity, we can assume that equations (45), (46), and (47) also hold when $\phi = \phi_c$. Setting $F = 0$ in equation (47) and using equation (45) gives the upper equilibrium filament current, J_u, and current sheet length, q_u

$$J_u = 2\sqrt{2}/\pi = 0.9003 , \tag{48}$$

$$q_u = h_u/\sqrt{3} . \tag{49}$$

Substituting these values into equation (46) gives the upper equilibrium height, h_u

$$h_u = \beta r^{-\alpha} , \tag{50}$$

where

$$\alpha = (\pi\sqrt{2}/4) - 1 = 0.1107 , \tag{51}$$

$$\beta = \frac{3}{2} 2^{\alpha} \exp\left[\frac{\pi\sqrt{2}}{4} - \frac{\sqrt{2}}{2} \tan^{-1}(2\sqrt{2})\right] = 2.0598 . \tag{52}$$

From equation (43) the stored magnetic energy at the lower equilibrium $h_0 = h_c = 1$ in the limit $r \to 0$ is

$$W_c = W_0 = \frac{I_0^2}{c^2} \ln\left(\frac{2}{r}\right) , \tag{53}$$

and the magnetic energy at the corresponding upper equilibrium h_u is

$$W_u = W_c - d \int_1^{h_u} F(h)\, dh . \tag{54}$$

Using equation (45) to eliminate q from equation (47) gives

$$F(h) = \frac{2I_0^2}{h\, dc^2} \left(\frac{J^2}{2} - \frac{4}{\pi^2}\right) , \tag{55}$$

and from equations (45) and (46) we get to lowest order in (r/h)

$$\ln(h) = (J^{-1} - 1) \ln(2/r) . \tag{56}$$

Thus

$$dh/h = -\ln(2/r) J^{-2}\, dJ , \tag{57}$$

and (54) becomes

$$W_u = W_c + \frac{2I_0^2}{c^2} \ln\left(\frac{2}{r}\right) \int_1^{J_u} \left(\frac{1}{2} - \frac{4}{\pi^2 J^2}\right) dJ , \tag{58}$$

where $J_u = 2(2)^{1/2}/\pi$. Upon integration, the energy at the upper equilibrium is

$$W_u = W_c - \frac{2I_0^2}{c^2} \left(\frac{1}{2} + \frac{4}{\pi^2} - \frac{2\sqrt{2}}{\pi}\right) \ln\left(\frac{2}{r}\right) . \tag{59}$$

The fractional change in magnetic energy when the filament moves from the lower equilibrium to the upper equilibrium is

$$\frac{W_u - W_c}{W_c} = \left(\frac{4\sqrt{2}}{\pi} - 1 - \frac{8}{\pi^2}\right) = 9.937 \times 10^{-3} . \tag{60}$$

Therefore, less than 1% of the available magnetic energy is released by the loss of mechanical equilibrium at the catastrophe point. The remaining 99% is locked up in the current sheet, and this energy can only be released by reconnection.

As the filament moves upwards beyond h_u, the magnetic energy starts to increase, and the filament reaches its upward maximum extension, h_m when the energy, W_m, becomes equal to the initial energy at h_c. Applying this condition gives the filament current, J_m, at the maximum extension, i.e.,

$$W_m - W_c = \frac{2I_0^2}{c^2} \ln\left(\frac{2}{r}\right) \int_1^{J_m} \left(\frac{1}{2} - \frac{4}{\pi^2 J^2}\right) dJ = 0 , \tag{61}$$

$$\frac{J_m}{2} + \frac{4}{\pi^2 J_m} - \frac{1}{2} - \frac{4}{\pi^2} = 0 , \tag{62}$$

$$J_m = \frac{8}{\pi^2} = 0.8106 . \tag{63}$$

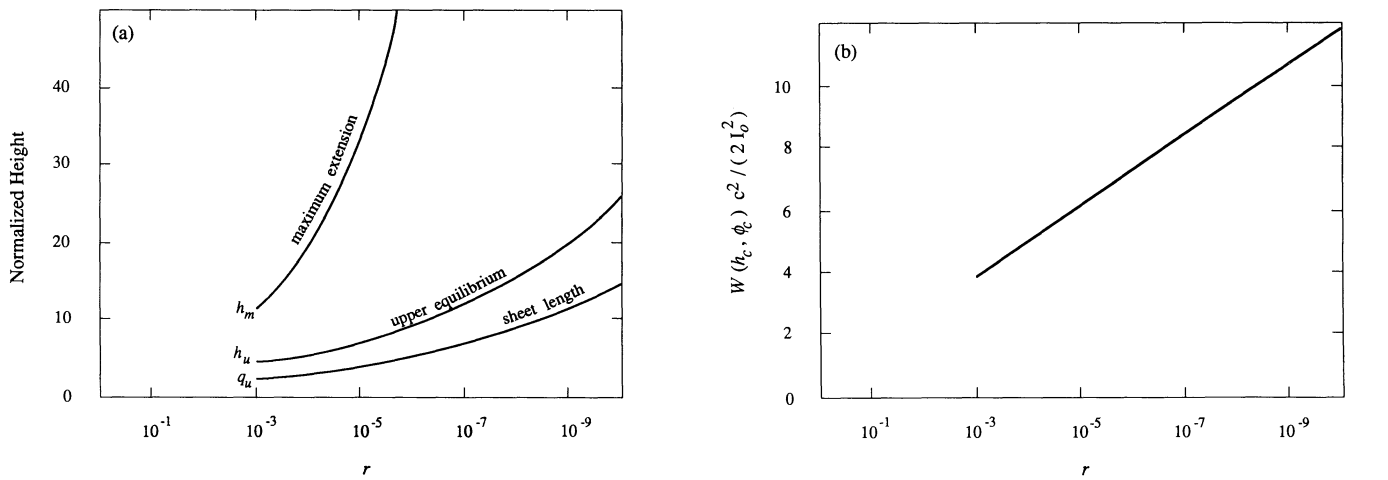

FIG. 9.—Asymptotic behavior at the critical flux, ϕ_c, as the filament radius r tends to zero. (*a*) Current sheet length, q_u, and filament heights, h_u and h_m, as functions of r. The quantities q_u and h_u refer to the upper equilibrium, while h_m refers to the maximum extension height. (*b*) Stored magnetic energy at the critical point, $W(h_c, \phi_c)$, as a function of r.

Substituting this value of J into equations (45) and (46) gives

$$h_m = \lambda r^{-\xi}\,, \tag{64}$$

where

$$\xi = \frac{\pi^2}{8} - 1 = 0.2337\,, \tag{65}$$

$$\lambda = 2^{\xi}\left(1 + \frac{\pi^2}{16}\right)\exp\left[\frac{\pi^2}{8} - \frac{\pi}{4}\tan^{-1}\left(\frac{8\pi}{16 - \pi^2}\right)\right] = 2.2941\,. \tag{66}$$

Figure 9 plots h_u, h_m, q_u, and W_0 as functions of the radius, r. Because of the logarithmic dependency of the solution on r, very large changes in r cause only minor changes in the catastrophe point values. For example, decreasing the radius by four orders of magnitude from 10^{-5} to 10^{-9} only increases the upper equilibrium filament height by a factor of 2.8 and the stored magnetic energy by a factor of 1.4.

Table 2 compares the asymptotic results with the numerical results. The close agreement between these results verifies that both our numerical and asymptotic procedures for solving the equations are correct.

7. PHYSICAL IMPLICATIONS

The analysis in the previous sections shows that catastrophe behavior does indeed occur in an ideal–MHD version of the Van Tend and Kuperus model. However, the ratio of the radius of the current filament to the length scale of the photospheric magnetic field has to be less than 10^{-3} to get this behavior in our particular model. In this section we consider whether such a small ratio is consistent with the observed properties of the solar atmosphere.

We can express the filament radius in terms of four parameters inferred from observations. These parameters are d, the length scale of the photospheric field; L, the length of the current filament; B_d, the strength of the photospheric field; and E, the total magnetic energy released during a CME. From equation (12) the vertical magnetic field at the photosphere is

$$B_y(x, 0) = -\frac{1}{d}\frac{\partial A}{\partial x} = \frac{2I_0}{cd}\frac{4x}{(x^2 + 1)^2}\,, \tag{67}$$

TABLE 2

COMPARISON OF NUMERICAL AND ASYMPTOTIC SOLUTIONS

Filament Radius r	Length/Height Ratio q_u/h_u		Upper Equilibrium Current J_u		Upper Equilibrium Height h_u		Upper Equilibrium Energy W_u	
	Num.	Asym.	Num.	Asym.	Num.	Asym.	Num.	Asym.
10^{-5}.....	0.512	0.577	0.922	0.900	4.90	7.37	6.114	6.042
10^{-7}.....	0.555	0.577	0.910	0.900	9.93	12.27	8.398	8.322
10^{-9}.....	0.571	0.577	0.904	0.900	18.4	20.42	10.677	10.602

and defining B_d as $B_d = B_y(1, 0)$, we find that the current I_0 is

$$I_0 = dcB_d/2 . \tag{68}$$

Therefore, from equation (53) the normalized radius r is approximately

$$r = 2 \exp [- 4E/B_d^2 Ld^2] \tag{69}$$

where we take $E = W_0 L$. We are also interested in the field at the surface of the filament which from equation (16) is approximately

$$B_s \equiv B_x(0, h - r) = B_d/r . \tag{70}$$

Choosing $B_d = 100$ G, $d = 10^4$ km, $L = 10^5$ km, and $E = 10^{32}$ ergs gives $B_s = 2.7 \times 10^3$ G and $r = 3.7 \times 10^{-2}$. This value of r corresponds to a filament radius of 370 km which is a plausible value, but our particular model no longer has catastrophic behavior when the radius is this large. Since r depends exponentially on the values of the parameters, it is relatively easy to get small radii by slightly altering the choice of values. For example, decreasing d by a factor of 2 gives $r = 6.8 \times 10^{-4}$ which corresponds to a filament radius of 3.4 km. But when the radius is 3.4 km, the field B_s at the surface of the filament is 1.5×10^5 G, and so it is hard to imagine that the filament radius could really be this small.

The problem with adjusting the radius to a plausible value stems from the logarithmic dependence of the flux upon the radius. The logarithmic dependence is a consequence of having only a two-dimensional model, and this dependence would no longer exist in a three-dimensional model. Thus, the need for a small radius may be an artifact of using only two dimensions.

It might also be possible to get catastrophe behavior at a larger radius by removing the assumption that the filament radius is constant. The assumption of constant radius is not very realistic since the filament should expand adiabatically when the current decreases during the eruption. When the filament radius expands, the decrease in current is not as great. Consequently, if a limiting radius still exists, then it must be larger than the limiting radius we have found here for an incompressible filament.

A small filament radius also aversely affects the requirements for storing enough magnetic energy in the corona to produce a catastrophe. We have taken the view that the filament current is generated by photospheric reconnection. This is not unreasonable since Martin, Livi, & Wang (1985) have observed a correlation between large flares and magnetogram features suggestive of photospheric reconnection. However, the amount of flux which must be reconnected in our particular model to reach the critical point is very much greater than the amount of reconnection implied by the Martin *et al.* (1985) observations. In the model, the initial flux in the photosphere is $4I_0/c$, but for $r = 10^{-3}$ the flux which must be reconnected to reach the sheet formation point is $13.2I_0/c$. Thus, to create the current sheet we need to reconnect about 3 times as much flux as exists in the photosphere initially.

In the model this flux is supplied by sources at $x = \pm\infty$, but such sources are not consistent with observations. However, if r were 0.1, the flux which would have to be reconnected to reach the sheet formation point would be only $4.0I_0/c$. Thus for this larger radius, the amount of flux which must be reconnected is of the same order as the amount of flux which exists in the photosphere initially, and there is no need for a large amount of flux to be transported in from $x = \pm\infty$. Even when the radius is small, it is still possible to avoid excessive reconnection by bringing the filament current up from below the photosphere. If this were done, then a small amount of reconnection would be sufficient to drive the system to the critical point.

8. CONCLUSIONS

We have confirmed that the catastrophe mechanism proposed by Van Tend & Kuperus (1978) still exists even in two-dimensional ideal MHD. By reconnecting fields in the photosphere one can increase the current in a pre-existing coronal current filament until the current becomes so strong that the balance between the magnetic compression and tension forces acting on the filament is suddenly lost. This sudden loss is a classic catastrophe that stretches the photospheric field upwards while releasing magnetic energy. However, in the absence of reconnection, the energy release is less than 1% of the stored magnetic energy.

In our particular model, no catastrophe occurs unless the filament radius is smaller than 10^{-3} times the length scale of the photospheric field. We estimate that the radius of a coronal current filament is unlikely to be this small, and therefore the model in its present form does not fit the observations. In constructing our model we have assumed that the filament radius is constant, and that the magnetic field is unsheared. By relaxing these assumptions, it may be possible to construct a model which does fit the observations.

This work was supported by the NASA grant NAGW-76 and NSF grant ATM-8916303 to the University of New Hampshire. The authors are grateful to P. Démoulin for his comments.

REFERENCES

Aly, J. J. 1984, ApJ, 283, 349
———. 1985, A&A, 143, 19
———. 1990, Computer Phys. Comm., 59, 13
Amari, T., & Aly, J. J. 1989, A&A, 208, 261
Anzer, U., & Ballester, J. J. 1990, A&A, 238, 365
Biskamp, D., & Welter, H. 1989, Solar Phys., 120, 49
Démoulin, P., & Priest, E. R. 1988, A&A, 206, 336
Forbes, T. G. 1990, J. Geophys. Res., 95, 11919
Forbes, T. G., & Priest, E. R. 1987, Revs. Geophys., 25, 1583
Hones, E. W., Jr. 1979, Space Sci. Rev., 23, 393
Kaastra, J. J. 1985, Ph.D. thesis, Rijksuniversiteit, Utrecht
Klimchuk, J. A., & Sturrock, P. A. 1989, ApJ, 345, 1034
Low, B. C. 1977, ApJ, 212, 234
———. 1981, ApJ, 251, 352
Martens, P. C. H., & Kuin, N. P. M. 1989, Solar Phys., 22, 263
Martin, S. F., Livi, S. H. B., & Wang, J. 1985, Australian J. Phys., 38, 929
Mikic, Z., Barnes, D. C., & Schnack, D. D. 1988, ApJ, 328, 830
Molodenskii, M. M., & Filippov, B. P. 1987, Soviet Astr. (English Translation), 31, 564
Priest, E. R., & Forbes, T. G. 1990, Solar Phys., 126, 319
Reitz, J. R., & Milford, F. J. 1960, Foundations of Electromagnetic Theory (Reading, MA: Addison-Wesley), p. 170
Sturrock, P. A. 1987, Solar Phys., 113, 13
———. 1989, Solar Phys., 121, 387
Syrovatskii, S. I. 1971, Soviet Phys. JETP Letters, 33, 933
van Ballegooijen, A. A., & Martens, P. C. H. 1989, ApJ, 343, 971
Van Tend, W. 1979, Solar Phys., 61, 89
Van Tend, W., & Kuperus, M. 1978, Solar Phys., 59, 115
Wagner, W. J., Hildner, E., House, L. L., Sawyer, C., Sheridan, K. V., & Dulk, G. A. 1981, ApJ, 244, L123
Wolfram, S. 1988, Mathematica: A System for Doing Mathematics by Computer (Reading, MA: Addison-Wesley), p. 478
Yeh, T. 1982, Solar Phys., 78, 287
———. 1983, ApJ, 264, 630
Yeh, T., & Axford, W. I. 1970, J. Plasma Phys., 4, 207